Proceedings of the ASME 34th International Conference on Ocean, Offshore and Arctic Engineering
OMAE2015
May 31-June 5, 2015, St. John's, Newfoundland, Canada

OMAE2015-41577

GENERATING AND ABSORBING BOUNDARY CONDITIONS FOR FREE-SURFACE FLOW SIMULATIONS IN OFFSHORE APPLICATIONS

Bülent Düz*
René H.M. Huijsmans
Department of Ship Hydrodynamics
Technical University of Delft
Mekelweg 2, 2628 CD Delft
The Netherlands
b.duz@academy.marin.nl
r.h.m.huijsmans@tudelft.nl

Peter R. Wellens
Mart J.A. Borsboom
Deltares
P.O. Box 177, 2600 MH Delft
The Netherlands
{mart.borsboom, peter.wellens}@deltares.nl

Arthur E.P. Veldman†
Roel Luppes
Institute for Mathematics and Computer Science
University of Groningen
P.O. Box 407, 9700 AK Groningen
The Netherlands
{a.e.p.veldman, r.luppes}@rug.nl

ABSTRACT

Numerical simulations of wave phenomena necessarily have to be carried out in a limited computational domain. This implies that incoming waves should be prescribed properly, and the outgoing waves should leave the domain without causing reflections. In this paper we will present an enhanced type of such generating and absorbing boundary conditions (GABC). The new approach is applied in studies of extreme hydrodynamic wave impact on rigid and floating structures in offshore and coastal engineering, for which the VOF-based CFD simulation tool ComFLOW has been developed.

INTRODUCTION

Since the 19th century when first wave theories were proposed, understanding the motion and behavior of the waves in nature has been a very popular subject among researchers from various fields of science. Typically the phenomena of interest are local but embedded in a vast spatial domain; for example, the interaction between free surface waves and numerous kinds of man-made structures in the ocean. For efficient computational modeling, this vast spatial domain around the region of interest is truncated via artificial boundaries, which suggests that a compact computational domain around the structure and a residual infinite domain are introduced. At this point, one of the most elusive and difficult topics surfaces when we try to answer this question: What is the boundary condition to be imposed on these artificial boundaries in such a way that the solution in the compact domain coincides with the solution in the original domain? In the literature the boundary conditions applied on the artificial boundaries are called by various names, such as non-reflecting, absorbing, open, transparent and radiating boundary conditions. Here, we will use the term Absorbing Boundary Condition (ABC).

Several types can be listed under the wide variety of ABCs: Nonlocal, semi-local or local operators, numerical dissipation zones and Dirichlet-to-Neumann (DtN) map based conditions. For a review regarding high-order local ABCs, see [1]. [2] and [3] present lengthy overviews of local and non-local ABCs along with other artificial boundary conditions. Also, [4] offers a survey of exact ABCs. [5] discusses the use of ABCs and numerical dissipation zones suitable especially for compressible turbulent shear flows. For a review of ABCs and PMLs for wave propagation problems, the reader is referred to [6]. Several techniques to absorb free surface waves are briefly discussed by [7].

In the paper we will present a new type of ABC, which are used in the ComFLOW project [8–10]. In this project a numerical CFD method is developed to simulate the hydrodynamic impact of extreme waves on offshore platforms and coastal constructions.

*Present address: MARIN, P.O. Box 28, 6700 AA, Wageningen, The Netherlands

†Address all correspondence to this author.

HIGHER-ORDER BOUNDARY CONDITIONS

For convenience we will present a short introduction to the first hierarchy of local absorbing boundary conditions developed by [11]. This work can be considered as one of the cornerstones in the field of absorbing boundary conditions, and is essentially related to the ABC that we will design. We start the discussion by considering the two dimensional wave equation

$$\frac{\partial^2\phi}{\partial t^2} = c^2\left(\frac{\partial^2\phi}{\partial x^2} + \frac{\partial^2\phi}{\partial y^2}\right), \tag{1}$$

where c is the propagation or phase speed. Solutions of this equation are plane waves which have the following form

$$\phi(x,y,t) = e^{i(k_x x + k_y y - \omega t)} \tag{2}$$

where ω is the frequency and (k_x, k_y) are the components of the wave number vector in the x- and y -directions, respectively, $k = (k_x, k_y)$. Substitution of Eq. (2) in Eq. (1) results in the following expression

$$\omega^2 = c^2(k_x^2 + k_y^2) \quad \Rightarrow \quad k_x = \frac{\omega}{c}\sqrt{1 - \left(\frac{k_y c}{\omega}\right)^2}, \tag{3}$$

which is called the dispersion relation.

The square root on the right-hand side is replaced by a Taylor series representation in order to obtain a partial differential equation which can be locally discretized in physical domain. Considering only the first few terms of its Taylor series representation we can approximate the square root as $\sqrt{1-s} = 1 - \frac{1}{2}s + O(s^2)$, where $s = (k_y c/\omega)^2$ (see [12] for a discussion on various expansion techniques). If we take only the first term in this representation and ignore the rest, hence $\sqrt{1-s} \approx 1$, and transform the resulting dispersion relation back into the physical domain, we obtain

$$-\omega + c k_x = 0 \quad \Rightarrow \quad \left(\frac{\partial}{\partial t} + c\frac{\partial}{\partial x}\right)\phi = 0. \tag{4}$$

Eq. (4) is the 1^{st}-order Engquist-Majda boundary condition [11], or alternatively the Sommerfeld condition [13]. In other terms, it shows that the ingoing characteristic variable should vanish. Similarly, if we consider the first two terms in the Taylor series representation and redo the process, we reach

$$\left(\frac{\partial}{\partial t} + c\frac{\partial}{\partial x}\right)^2 \phi = 0. \tag{5}$$

which is the 2^{nd}-order Engquist-Majda boundary condition. The order can be increased further in a similar way.

Higdon [14, 15] showed that it is possible to allow the wave under an angle of incidence α with the outflow boundary; in the higher-order conditions even more angles can be chosen: $\alpha_p,\ p = 1, \ldots, P$, where P is the order of the boundary condition. Higdon's condition reads:

$$\prod_{p=1}^{P}\left(\cos\alpha_p \frac{\partial}{\partial t} + c\frac{\partial}{\partial x}\right) = 0 \tag{6}$$

In order to assess the benefit of using Eq. (6) as opposed to Eq. (4), we need to take a look at the amount of spurious reflection generated by each scheme as a function of the angle of incidence. For this purpose, at the artificial boundary the solution can be expressed as the sum of the outgoing and reflected waves, that is

$$\phi(x,y,t) = e^{i(k_x x + k_y y - \omega t)} + R\, e^{i(-k_x x + k_y y - \omega t)}, \tag{7}$$

where the first term represents the wave with amplitude equal to unity impinging on the boundary, and the second term represents the spuriously reflected wave with amplitude R. To evaluate R, we substitute Eq. (7) into the general Higdon boundary conditions Eq.(6), and arrive at the following relation

$$|R_H| = \prod_{p=1}^{P}\left|\frac{\cos\alpha_p - \cos\theta}{\cos\alpha_p + \cos\theta}\right|, \tag{8}$$

where θ is the 'real' angle of incidence measured in the clockwise or counter-clockwise direction from the positive x-direction, $|\theta| < \pi/2$. Observing Eq. (8), it can be readily seen that Higdon's boundary conditions is nonreflecting as soon as θ equals one of the $\pm\alpha_p$'s in combination with a wave speed c.

In addition to directional effects of the waves, dispersion has also been the focus of many researchers. Considering the highly nonlinear governing equations which are employed in many complex modeling applications, it is unlikely to have a priori knowledge regarding the phase speed c. As a result c is generally computed during the course of the numerical simulation. Orlanski [16] suggested the following idea to compute c as $c = -(\partial\phi/\partial t)/(\partial\phi/\partial x)$. Clearly, this expression is found from the boundary conditions (4) itself, and makes sense only in the discrete form. To discretize the right-hand side, he suggested using the information near the boundary at the previous time step via suitable finite difference approximations. An obvious problem is that we may encounter unphysical values from this computation. When the angle of incidence increases, i.e., the waves are rather oblique, the normal derivative approaches zero, which

results in an infinitely large value for c. Furthermore, if $c < 0$ is obtained, then this implies that information propagates back into the domain instead of outside. Thus much 'safeguarding' procedures have to be built in to prevent numerical instabilities. For a survey the reader is referred to [17] and [18].

DERIVATION OF THE ABC

In ComFLOW, the equations of motion are solved in a computational domain Ω (see Fig. 1) via imposing various types of boundary conditions such as free surface, wall, inflow and absorbing boundary conditions. Typically on the west and south boundaries Γ_W and Γ_S the incoming wave is prescribed. At every time level starting from $t = 0$, free surface elevations, values of the velocity components and pressure corresponding to the considered wave model are provided on Γ_W and Γ_S. At the bottom Γ_B we specify a no-slip no-penetration condition which is simply the Dirichlet condition.

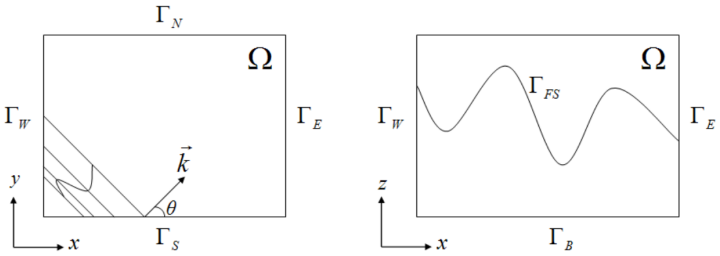

FIGURE 1. A COMPUTATIONAL DOMAIN WITH Γ_N AND Γ_E AS ARTIFICIAL BOUNDARIES.

At the free surface Γ_{FS} the continuity of normal and tangential stresses results in expressions for the velocity components and pressure. In-depth analysis of how these equations are implemented is beyond the scope of this paper. We now introduce two artificial boundaries Γ_N and Γ_E , see Fig. 1. To complete the statement of the problem, we will implement an ABC on these artificial boundaries.

ABC-1 (Dispersive ABC)

Consider the 1^{st}-order version of Higdon's boundary operator (6) and replace c by the familiar dispersion relation

$$c = \sqrt{gh}\sqrt{\frac{\tanh(kh)}{kh}}, \tag{9}$$

then we obtain

$$\left(\cos\alpha\,\frac{\partial}{\partial t} + \sqrt{gh}\sqrt{\frac{\tanh(kh)}{kh}}\,\frac{\partial}{\partial x}\right)\phi = 0. \tag{10}$$

Each individual component of this wave has its own frequency, amplitude, wave number and phase. Therefore, the boundary condition (10) cannot annihilate all these wave components, simply because it is evidently designed for only one of them.

At this point a question crosses one's mind: Is it possible to develop a boundary condition which has the feature of allowing reflection only to an acceptable threshold for all the components which all together form an irregular wave? One can deduce from the way this question is asked that we expect some amount of reflection for such a boundary condition, but it will be restricted within certain limits.

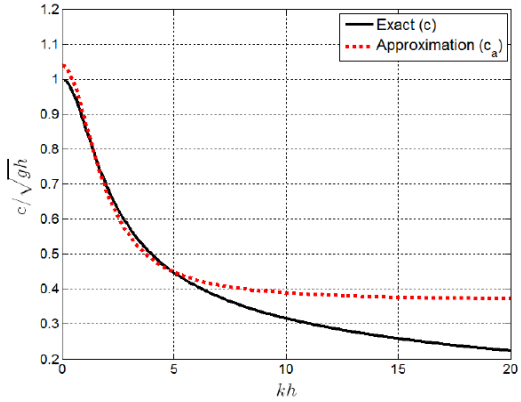

FIGURE 2. APPROXIMATION OF THE DISPERSION RELATION. FOR THE COEFFICIENTS IN (11), $a_0 = 1.04$, $a_1 = 0.106$ AND $b_1 = 0.289$ ARE USED.

Now we introduce the following rational expression which approximates the dispersion relation (9),

$$c_a = \sqrt{gh}\frac{a_0 + a_1(kh)^2}{1 + b_1(kh)^2}, \tag{11}$$

where a proper choice of coefficients a_0 , a_1 and b_1 leads to a close approximation for the largest possible range of kh values, see Fig. 2. The difference between the two curves gives an indication for the amount of reflection caused by the rational approximation. Now a further improvement is introduced into the design of the boundary condition: by exploiting the exponential behavior of the wave potential in the z-direction. The wave number k is computed locally from the potential itself, via

$$k^2\phi = \frac{\partial^2}{\partial z^2}\phi. \tag{12}$$

This relation can be substituted into (11) and combined with (10)

to reach the final form of the absorbing boundary condition at Γ_E

$$\cos\alpha\left(1+b_1h^2\frac{\partial^2}{\partial z^2}\right)\frac{\partial\phi}{\partial t}+\sqrt{gh}\left(a_0+a_1h^2\frac{\partial^2}{\partial z^2}\right)\frac{\partial\phi}{\partial x}=0. \tag{13}$$

Following the same method, it is easy to write the ABC on Γ_N.

ABC-2 (Dispersive Directional ABC)

Now, a further modification of the dispersive ABC will be discussed to account for both dispersive and directional effects of the waves. As the 2^{nd}-order Higdon ABC has superior performance over the 1^{st}-order one in terms of directional effects, we will incorporate the improvements that we made in the previous section concerning dispersive effects. As this ABS consists of the product of two operators, and considering the relations (11) and (12), we realize that only one of the operators can include the approximation for the dispersion relation. Otherwise, the product of two approximations would yield a fourth-order derivative in the z-direction which will cause difficulties when discretized at the boundaries. Therefore, we substitute the relations (11) and (12) in one of the operators. The resulting expression for the 2^{nd}-order ABC-2 is the following

$$\left(\cos\alpha_1\frac{\partial}{\partial t}+c\frac{\partial}{\partial x}\right)\left[\cos\alpha_2\left(1+b_1h^2\frac{\partial^2}{\partial z^2}\right)\frac{\partial\phi}{\partial t}+\sqrt{gh}\left(a_0+a_1h^2\frac{\partial^2}{\partial z^2}\right)\frac{\partial\phi}{\partial x}\right]=0\ . \tag{14}$$

Analogous with the discussion for the ABC-1, this expression can also be easily written for the boundary operator to be applied on Γ_N .

Reflection coefficients

Similar as above, reflection coefficients can be derived when angle of incidence and wave speeds vary. For the first order ABC (13) the reflection coeffient for a wave with incidence θ and an outgoing wave speed c^{out} reads

$$R=-\frac{c^{out}\cos\alpha_1-c_a\cos\theta}{c^{out}\cos\alpha_1+c_a\cos\theta}, \tag{15}$$

with c_a given by (11). A similar expression can be obtained for the second-order condition (14).

The difference in reflection coefficients as a function of the angle of incidence θ for the special case of a prescribed wave speed, i.e. $c_{out}=c_a=c$, is presented in Fig. 3. Here the angle-parameters in the ABC-1 and ABC-2 have been chosen as $\alpha=0^\circ$ for ABC-1, and $\alpha_1=0^\circ$, $\alpha_2=60^\circ$ for ABC-2. The superiority of ABC-2 over ABC-1 is immediately visible.

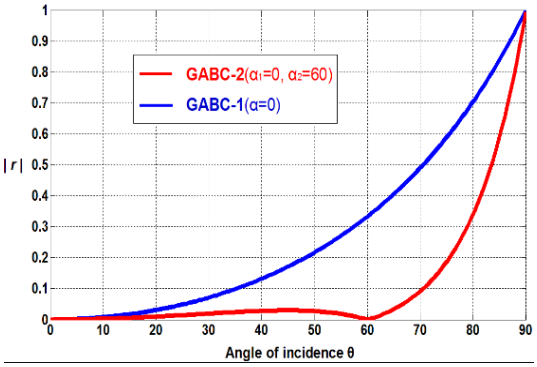

FIGURE 3. REFLECTION COEFFICIENTS FOR ABC-1 ($\alpha=0$) vs ABC-2 ($\alpha_1=0,\ \alpha_2=60^\circ$) FOR A GIVEN WAVE SPEED AS A FUNCTION OF THE ANGLE OF INCIDENCE.

If we take the approximative wave speed c_a from (11) into account, the assessment also has to include the choice of the wave numer. Figure 4 demonstrates the amount of reflection as a function of the angle of incidence θ and the dimensionless wave number kh to compare the effectiveness of the four boundary conditions; the 1^{st}-order and 2^{nd}-order Higdon operators, ABC-1 (with $\alpha=0^\circ$) and ABC-2 (with $\alpha_1=0^\circ$ and $\alpha_2=60^\circ$). For the coefficients in (11) we take $a_0=1.04$, $a_1=0.106$ and $b_1=0.289$ while respecting the stability limits concerning these coefficients [19] and providing a good approximation for the kh values from 0 to 20. We take $c^{out}=c=0.316\sqrt{gh}$; a choice which corresponds to the kh value of 10 which is in the middle of the considered kh-range between 0 and 20. All the angle parameters in the boundary conditions are set to be zero as an arbitrary initial choice.

In Fig. 4, light-colored areas between isolines illustrate small reflection zones, while as the color gets darker the amount of reflection increases since grazing incidence is approached where waves propagate parallel to the outflow boundary. More particularly, white-colored zones demonstrate the ranges where the reflection coefficient is below five percent, which is an acceptable threshold in practical wave simulations. The Higdon-conditions have been used with a c corresponding to $kh=10$, which is in the middle of the interval of interest. Note that in Fig. 4(a) for $\theta=0^\circ$, the minimum refelction coefficient indeed is obtained at $kh=10$. These results clearly show that the ABC-1 and ABC-2 cover a much wider kh-range of accurately absorbed waves than the 1^{st}- and 2^{nd}-order Higdon operators.

From ABC to GABC (Generating and Absorbing BC)

Sometimes it is necessary to radiate out an outgoing wave while allowing an incoming wave to propagate into the domain through the same boundary. A boundary treatment which provides such feature becomes a fully transparent boundary condition which is also referred to as Open Boundary Condition (OBC) in the literature [20, 21]. In order to preserve consistency

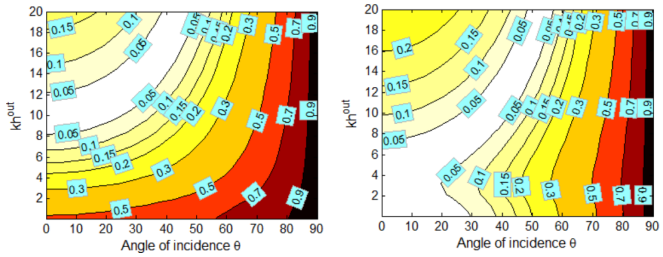

(a) First-order Higdon (6)

(b) First-order GABC (13)

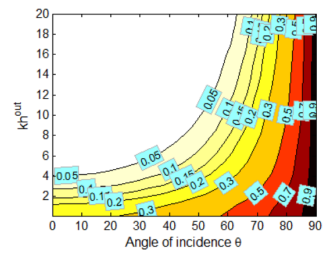

(c) Second-order Higdon (6)

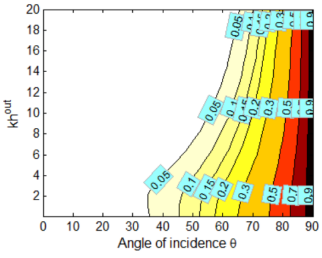

(d) Second-order GABC (14)

FIGURE 4. AMOUNT OF REFLECTION (IN PERCENT) AS A FUNCTION OF THE ANGLE OF INCIDENCE θ AND kh WHEN VARIOUS BOUNDARY CONDITIONS ARE USED. REFLECTION VALUES ARE WRITTEN ON THE CONTOUR LINES.

with the previous work in this field throughout the ComFLOW project, we will refer to it as Generating and Absorbing Boundary Condition (GABC). Carpenter [28] proposed such a method:

$$\left(\frac{\partial}{\partial t}+c\frac{\partial}{\partial x}\right)\phi=\left(\frac{\partial}{\partial t}+c\frac{\partial}{\partial x}\right)\phi^{in}. \qquad (16)$$

Here ϕ^{in} is the external function which is known a priori and x is the outward normal direction to the boundary where the condition is applied. This boundary condition has been used by a number of researchers including [21–24]. [25] used the same idea in the SKYLLA code which was developed at Delft Hydraulics. A brief discussion of the method was also presented by [20,26,27].

The fact that [28] used the same Sommerfeld operator on each side of the equation is simple and appealing. However, the Sommerfeld operator has strict limitations which effectively render the Carpenter scheme (16) low order accurate. [21] analyzed scheme (16) for the one-dimensional linear shallow water equations. Later, the accuracy was improved by replacing the Sommerfeld operator with the high-order Hagstrom-Warburton operator [29] for non-dispersive uniform [30] as well as non-uniform [31] media. [19] improved scheme (16) in terms of dispersive effects by replacing the phase speed c with Eqs. (11) and (12), and called the boundary condition GABC. The GABC allows long-crested dispersive waves to propagate in and out through the same boundary as long as the range of accuracy of Eq. (11) is respected.

In this study we improve the GABC further by implementing Eqs. (11) and (12) into the Higdon operators instead of the Sommerfeld operator. Hence we will use the ABC-1 or ABC-2 in the Carpenter scheme (16), and design a boundary condition which will account for short-crested dispersive waves traveling in and out of the computational domain over the same boundary.

RESULTS OF SIMULATIONS

In this section we present the results of the numerical experiments where the ABCs are applied at the outflow boundaries of the computational domain. In the first test, we will investigate the capability of the ABCs to account for only dispersive effects of the waves, and in the second test for only directional effects. In the third test, the ABCs will show a performance in terms of both when we will generate a short-crested wave in the computational domain.

The results of the numerical simulations will be analyzed through error norms. For that purpose, we introduce three error measures,

$$e(i,j)=\eta_s(i,j)-\eta_r(i,j),\ e_\Omega\equiv||e||_2 \text{ and } ||e||_\infty, \qquad (17)$$

where η is the free surface elevation. The subscript s indicates the solution in the domain of interest or 'small domain' and the subscript r indicates the reference solution. In the numerical experiments considered here, the reference solution is either obtained by solving the problem in a much larger domain with the same discretization in space and time or from analytical results. More information on the setup of the tests is given below. The common property of the global L_2-norm e_Ω (also used by [32]) and the infinity norm $||e||_\infty$ is that they display a complete picture of the error behavior in a single plot.

Dispersive properties of the ABCs

We apply the discrete ABCs to a problem in a two-dimensional computational domain where a linear regular wave is traveling along the x-direction. The wave has a period of $T=4s$ and a wave height of $H=0.1m$. With this wave we choose four different water depths, which produces four different kh values: 5, 10, 15 and 20. The parameters in the ABCs are not tuned for a particular kh value, rather they are fixed such that the reflection coefficient is minimum for the range of kh values between 0 and 20. Therefore, this test becomes especially useful to investigate the dispersive character of the boundary conditions. Here we employ the values given in Fig. 4. The length of the long domain is arranged in such a way that the reflected waves can not pollute the solution in the small domain. This allows us to use the solution in the long domain as a reference solution.

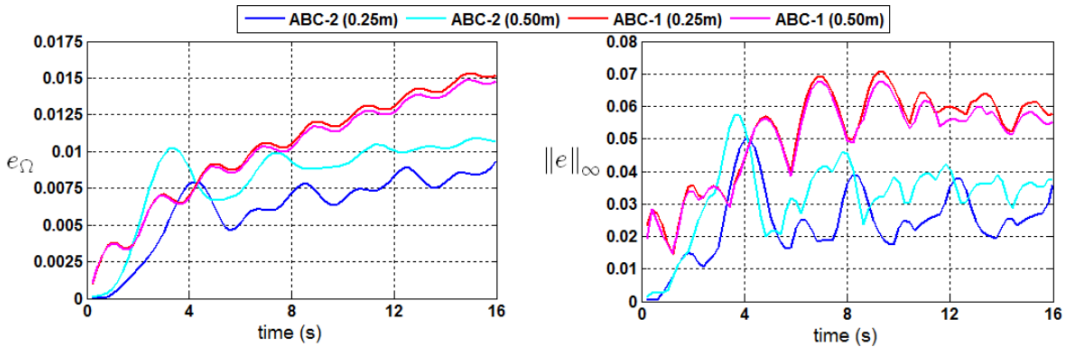

(a) $kh = 5$

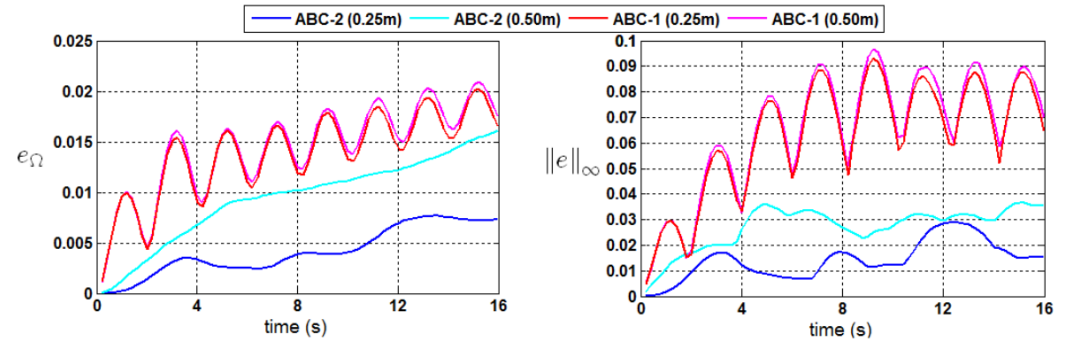

(b) $kh = 10$

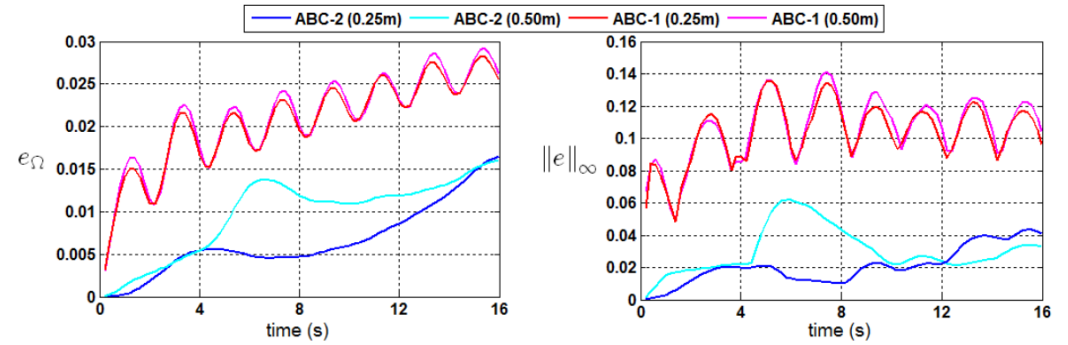

(c) $kh = 15$

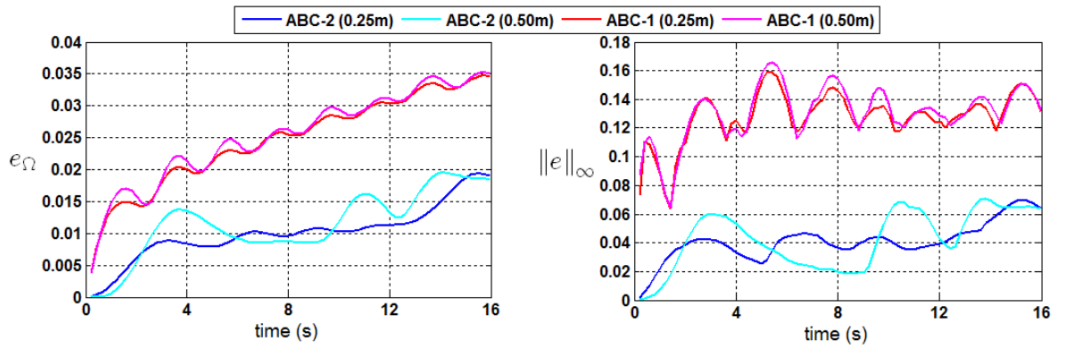

(d) $kh = 20$

FIGURE 5. ERROR NORMS FROM THE TWO ABCs IN A TWO-DIMENSIONAL DOMAIN ON TWO GRID RESOLUTIONS FOR WAVES WITH VARIOUS kh VALUES: FROM TOP TO BOTTOM: $kh = 5$, $kh = 10$, $kh = 15$ AND $kh = 20$.

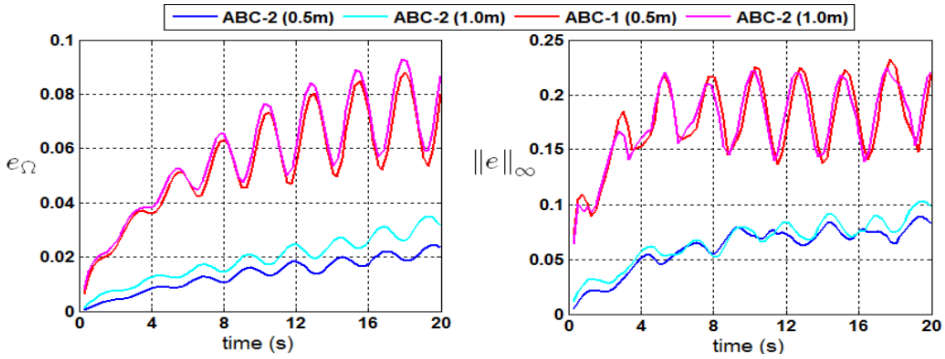

(a) $\theta = 20°$

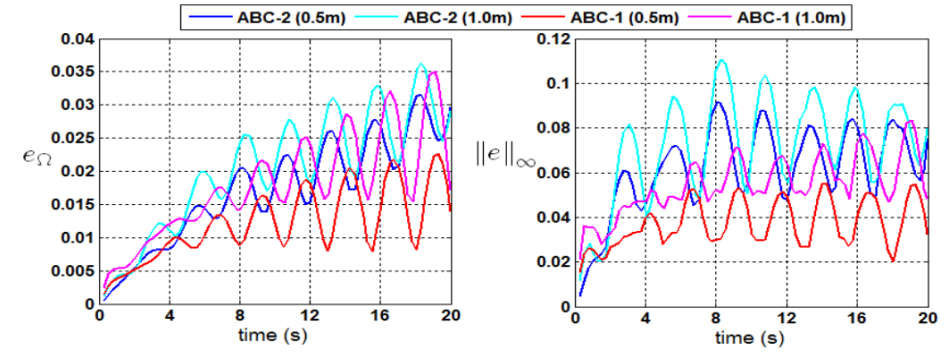

(b) $\theta = 40°$

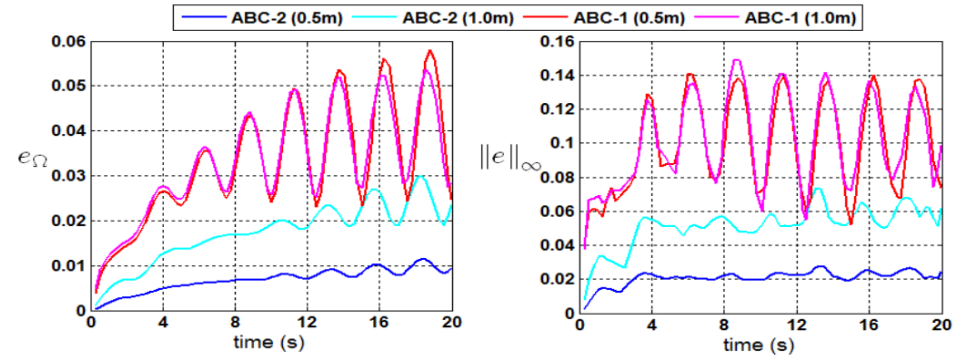

(c) $\theta = 60°$

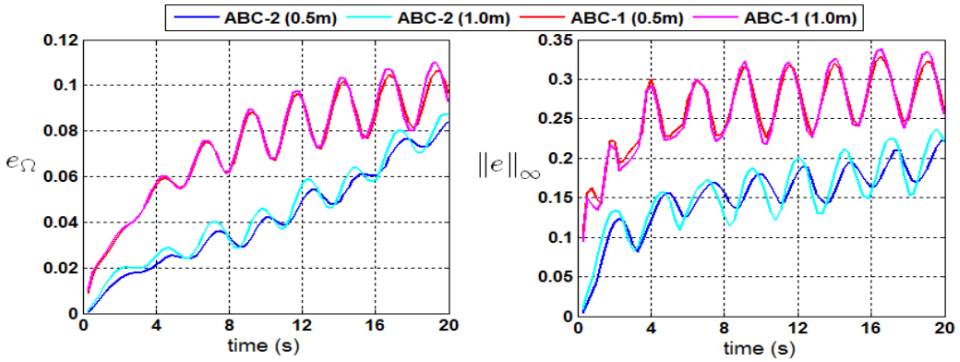

(d) $\theta = 80°$

FIGURE 6. ERROR NORMS FROM THE TWO ABCs ON TWO GRID RESOLUTIONS FOR WAVES WITH VARIOUS ANGLES OF INCIDENCE. FROM TOP TO BOTTOM RESULTS ARE SHOWN FOR $\theta = 20°$, $\theta = 40°$, $\theta = 60°$ AND $\theta = 80°$.

The results are shown in Fig. 5 on two grid resolutions. Errors are measured for a duration of $t_{max} = 16s$ which corresponds to four wave periods. Both error measures are normalized by the wave height. Results indicate that as kh values increase, the amount of reflection generated by ABC-1 increases from 7% for $kh = 5$ to nearly 16% for $kh = 20$; see the infinity norm $||e||_\infty$ in Fig. 5. The amount of reflection due to the use of the ABC-1 is characterized by the approximation that we applied for the dispersion relation. As shown in Fig. 2 this approximation becomes poorer as kh increases, which corresponds to an increase in reflection. On the other hand, the largest value of $||e||_\infty$ changes between 4% and 8% when ABC-2 is used. This is slightly higher than the maximum theoretical reflection coefficient illustrated in Fig. .

When the grid is refined, the results from ABC-1 change only kh slightly. With ABC-2 the change varies for different kh values: the infinity norm decreases 1% for $kh = 5$, 0.5% for $kh = 10$, 4% for $kh = 15$ and 2% for $kh = 20$. Also the global norm displays different amounts of improvement with grid refinement. Examining the discrete forms of the ABCs reveals that ABC-2 is more sensitive to grid refinement as it contains more spatial and temporal derivative terms.

Directional properties of the ABCs

Similar to the previous test case, the size of Ω_L is defined in such a way that the reflected waves from the outflow boundaries, which are located at $x = 230m$ and $y = 230m$, do not reach Ω_S during the simulation. At $t = 0s$, a fully developed linear regular wave is generated in both domains. At each time level, the numerical solution in Ω_S is compared to the reference solution in Ω_L . In both domains all numerical parameters are the same. Therefore, we can attribute the difference between the two solutions only to the performance of the ABCs at the outflow boundaries of Ω_S .

In this test we consider a wave which has a period of $T = 5s$ and a wave height of $H = 0.1m$. The water depth is $h = 5.75m$. With this wave we choose four different angles of incidence: $\theta = 20^\circ$, $\theta = 40^\circ$, $\theta = 60^\circ$ and $\theta = 80^\circ$, all of which are measured in the counter-clockwise direction from the positive x-axis. Similar to the previous test, the parameters of the ABCs will be kept constant for the four waves, thus the ABCs will not be tuned for a particular angle. The parameters are chosen in such a way that the reflection coefficient is minimum for the four angles of incidence. Thus we set $\alpha = 45^\circ$ for the ABC-1, and $\alpha_1 = 20^\circ$ and $\alpha_2 = 60^\circ$ for the ABC-2. The parameter c in the ABCs is chosen equal to the phase speed of the generated wave so that reflection is produced only by directional effects.

Figure 6 illustrates the global norm e_Ω and the infinity norm $||e||_\infty$ on two grid resolutions. Errors are measured for a duration of $t_{max} = 20s$ which corresponds to four wave periods. Both error measures are normalized by the wave height. Results indicate that ABC-1 produces the smallest reflection for the case with $\theta = 40^\circ$, i.e., the value of $||e||_\infty$ is around 5% on the fine grid. This is expected since in this case θ is closest to $\alpha = 45^\circ$. As the angle of incidence differs more from α, reflection increases. $||e||_\infty$ has the values of 14% at $\theta = 60^\circ$, 23% at $\theta = 20^\circ$ and 33% at $\theta = 80^\circ$ from the ABC-1 on the fine grid. With the ABC-2 reflection is the smallest when θ is close to α_1 or α_2 . This is also consistent with the theoretical reflection behavior; see Fig. 3. $||e||_\infty$ has the values of 8% at $\theta = 20^\circ$, 3% at $\theta = 60^\circ$, 9% at $\theta = 40^\circ$ and 23% at $\theta = 80^\circ$ from the ABC-2 on the fine grid.

This demonstrates the relative strength of the ABC-2 compared to ABC-1 in terms of directional effects of the waves.

Directional irregular wave test

In this final experiment, the ABCs are applied in a computational domain where a directional irregular wave is generated. Similar to the previous cases the reference solution used in the error measures is computed by solving the problem in a vast domain Ω_L which is larger than the small domain Ω_S only in the x-y plane, see Fig. 7 for the illustration of the problem. Before, we showed the performances of the ABCs concerning the dispersive and directional effects of the waves separately. Here we combine the two effects and produce a test where the wave is composed of a large number of components each with its own propagation direction, which naturally resembles practical situations in a better way. In the previous numerical experiments we had the information regarding the phase speed and angle of incidence beforehand. In this case we do not know the phase speed or the angle of incidence of the component which is impinging on the outflow boundaries. Therefore we will choose the parameters in the ABCs in such a way that the reflection coefficient is minimum for the ranges of kh and θ of the components.

The free surface of the directional irregular wave with 537

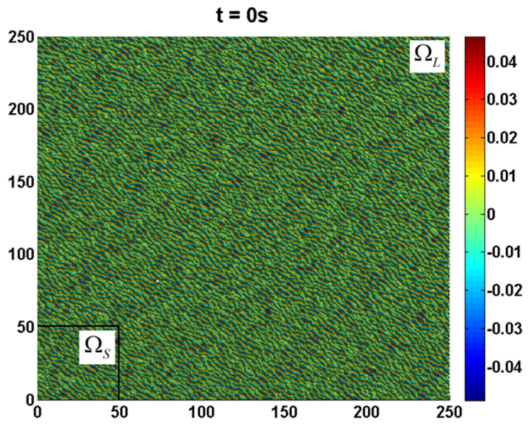

FIGURE 7. THE SETUP FOR THE DIRECTIONAL IRREGULAR WAVE SIMULATION.

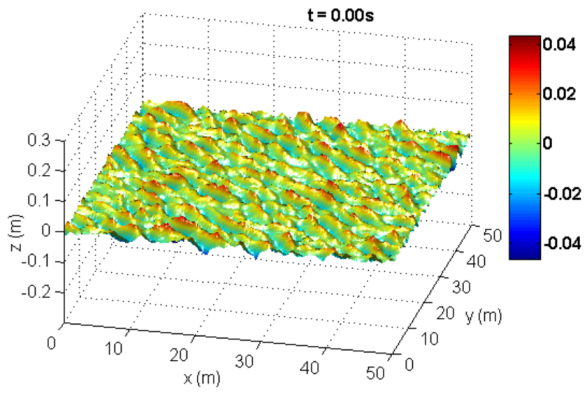

FIGURE 8. THE INITIAL CONDITION FOR THE DIRECTIONAL IRREGULAR WAVE SIMULATION.

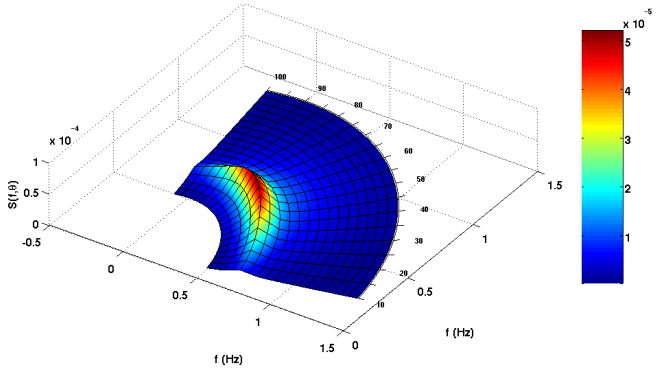

FIGURE 9. THE DIRECTIONAL SPECTRUM OF THE IRREGULAR WAVE.

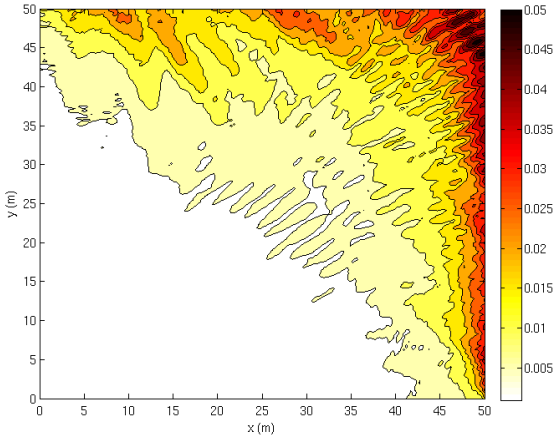

(a) Pointwise error for ABC-1

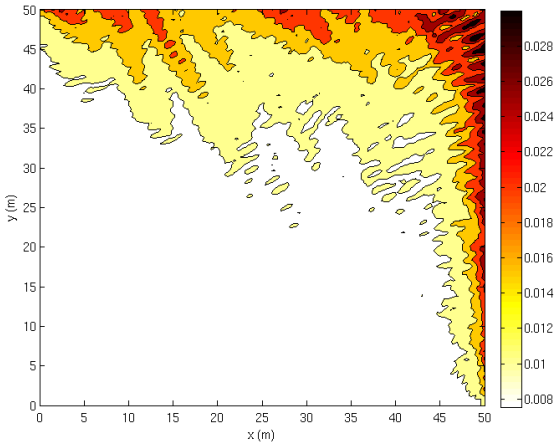

(b) Pointwise error for ABC-2

FIGURE 10. THE POINTWISE ERROR $|e|_\infty$ AVERAGED OVER TIME FOR THE TESTS WITH ABC-1 AND ABC-2. THE ERROR HAS BEEN SCALED WITH THE AVERAGE WAVE HEIGHT $H_s = 0.1\,\mathrm{m}$ (NOTE THE DIFFERENT COLOR SCALE).

Fourier components is shown in Fig. 8. A JONSWAP spectrum wave (Fig. 9) with $T_p = 9s$ and $H_s = 0.1m$ is simulated by performing 4000 time-steps at $\Delta t = 0.009s$. The lengths of Ω_S in the x- and y-directions are the same, $l_x = l_y = 50m$, and the water depth is $h = 2.875m$. By running the simulations for $t_{max} = 36.0s$ and taking into account the phase speed of the fastest propagating wave component $\sqrt{gh}$, we calculate the lengths of Ω_L in the x- and y-directions as $L_x = L_y = 250m$. Two uniform grid resolutions are considered: $0.5m$ and $0.25m$.

Figure 10 shows the pointwise error $|e(i,j)|$ from (17), normalized with H_s, as a function of space but averaged over time. As was to be expected, the largest errors occur near the outflow boundaries. Also, it is imminent that the second-order ABC-2 is significantly better than its first-order counterpart ABC-1 (note the difference in color scale).

Figure 11 shows the global L_2-norm e_Ω and the infinity norm $||e||_\infty$ as a function of time on two grid resolutions for the two ABCs. The largest value of $||e||_\infty$ for the ABC-1 is nearly 21.0%, whereas it is only 11.0% with the ABC-2. $||e||_\infty$ demonstrates a highly erratic behavior with ABC-1: it reaches the value of 11.0% at $t = 12.0s$, changes to 21.0% at $t = 23.0s$, and decreases back to 9.0% at $t = 30.0s$. When it comes to ABC-2, however, it oscillates within a much more limited band of 7.0% to 11.0% during the entire simulation.

CONCLUSIONS

The paper presents a new class of generating and absorbing boundary conditions (GABC). It is based on the well-known conditions of Sommerfeld [13], Engquist-Majda [11] and Hig-

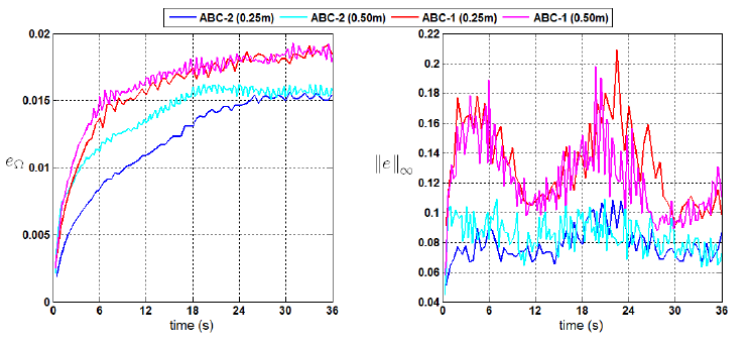

FIGURE 11. ERROR NORMS e_Ω AND $||e||_\infty$ AS A FUNCTION OF TIME FROM THE TWO ABCs ON TWO GRID RESOLUTIONS.

don [15]. The innovative aspect is that the wave speed featuring in these conditions, which is usually unknown due to dispersion, is determined from the local flow solution. The performance of these absorbing boundary conditions has been demonstrated a.o. for dispersive waves under varying angles of incidence. The test problems include a case with directional, irregular dispersive waves. The second-order variant ABC-2 clearly outperforms the first-order variant ABC-1.

ACKNOWLEDGMENT

The research is supported by the Dutch Technology Foundation STW, applied science division of NWO and the technology programma of the Ministry of Economic Affairs in The Netherlands (contracts GWI.6433 and 10475).

REFERENCES

[1] Givoli, D., 2004. "High-order local non-reflecting boundary conditions: a review". *Wave Motion*, **39**, pp. 319–326.

[2] Givoli, D. 1991. "Non-reflecting boundary conditions". *J. Comput. Phys.*, **94**, pp. 1–29.

[3] Tsynkov, S.V., 1998. "Numerical solution of problems on unbounded domains. A review". *Appl. Numer. Math.*, **27**, pp. 465–532.

[4] Hagstrom, T., 1999. "Radiation boundary conditions for the numerical simulation of waves". *Acta Numer.*, **8**, pp. 47–106.

[5] Colonius, T., 2004. "Modeling artificial boundary conditions for compressible flow". *Annu. Rev. Fluid Mech.*, **36**, pp. 315–345.

[6] D. Appelö, D., 2003. *"Non-reflecting boundary conditions for wave propagation problems"*. PhD thesis, Royal Institute of Technology, Sweden.

[7] Romate, J.E., 1992. "Absorbing boundary conditions for free surface waves". *J. Comput. Phys.*, **99**, pp. 135–145.

[8] Duz, B., Huijsmans, R.H.M., Wellens, P.R., Borsboom, M.J.A. and Veldman, A.E.P., 2012. "Application of an absorbing boundary condition in a wave-structure interaction problem". In *Proceedings of the 31st Int. Conf. on Ocean, Offshore and Arctic Eng. OMAE2012*, **5**, pp. 863–872.

[9] Duz, B., Huijsmans, R.H.M., Veldman, A.E.P., Borsboom, M.J.A. and Wellens, P.R., 2013. "An absorbing boundary condition for regular and irregular wave simulations". in: L. Eça, E. Oñate, J. Garcia-Espinosa, T. Kvamsdal and P. Bergan (Eds.), *Computational Methods in Applied Sciences*, **29**, Springer, pp. 31–45.

[10] Veldman, A.E.P., Luppes, R., van der Heiden, H.J.L., van der Plas, P., Düz, B. and Huijsmans, R.H.M., 2014. "Turbulence modeling, local grid refinement and absorbing boundary conditions for free-surface flow simulations in offshore applications". *33rd Int. Conf. on Ocean, Offshore and Arctic Engng*, San Francisco, 8-13 June, 2014. Paper OMAE2014-24427.

[11] Engquist, B. and Majda, A., 1977. "Absorbing boundary conditions for the numerical simulation of waves". *Math. Comput.*, **31**, pp. 629–651.

[12] Renaut, R.A. and Parent, J.S., 1996. "Rational approximations to $\sqrt{1-s^2}$, one-way wave equations and absorbing boundary conditions". *J. Comput. Appl. Math*, **72**, pp. 245–259.

[13] [1] Sommerfeld, A., 1949. *"Partial differential equations in physics"*. Academic Press.

[14] Higdon, R.L., 1986. "Absorbing boundary conditions for difference approximations to the multi-dimensional wave equation". *Math. Comput.*, **47**, pp. 437–459.

[15] Higdon, R.L., 1987. "Numerical absorbing boundary conditions for the wave equation". *Math. Comput.*, **49**, pp. 65–90.

[16] Orlanski, I., 1976. "A simple boundary condition for unbounded hyperbolic flows". *J. Comput. Phys.*, **21**, pp. 251–269.

[17] Hedley, M. and Yau, M.K., 1988. "Radiation boundary conditions in numerical modeling". *Mon. Wea. Rev.*, **116**, pp. 1721–1736.

[18] Jensen, T.G., 1998. "Open boundary conditions in stratified ocean models". *J. Marine Syst.*, **16**, pp. 297–322.

[19] Wellens, P., 2012. *"Wave simulation in truncated domains for offshore applications"*. PhD Thesis, Delft University of Technology, The Netherlands.

[20] Blayo, E. and Debreu, L., 2005. "Revisiting open boundary conditions from the point of view of characteristic variables". *Ocean Model.*, **9**, pp. 231–252.

[21] Mar-Or, A. and Givoli, D., 2006. "The global-regional model interaction problem: Analysis of Carpenter's scheme and related issues". *Int. J. Multiscale Comput. Eng.*, **4**, pp. 617–645.

[22] Bougeault, P., Mascart, J. and Chaboureau, J.P., 2013.

"The Meso-NH Atmospheric Simulation System: Scientific Documentation". Rapport technique, Centre National de Recherches Météorologiques (Météo-France) and Laboratoire d'Aérologie (CNRS).

[23] Perkins, A.L., Smedstad, L.F., Blake, D.W., Heburn, G.W. and Wallcraft, A.J., 1997. "A new nested boundary condition for a primitive equation ocean model". *J. Geophys. Res.*, **102**, pp. 3483–3500.

[24] Redelsperger, J.L. and Lafore, J.P., 1988. "A three-dimensional simulation of a tropical squall line: Convective organization and thermodynamic vertical transport". *J. Atmos. Sci.*, **45**, pp. 1334–1356.

[25] Van der Meer, J.W., Petit, H.A.H., van den Bosch, P., Klopman, G. and Broekens, R.D., 1992. "Numerical simulation of wave motion on and in coastal structures". In *Proceedings of the 23rd Int. Conf. on Coastal Engineering*, **2**, pp. 1772–1784.

[26] Durran, D.R., 2010. *"Numerical methods for fluid dynamics with applications to geophysics"*. Springer.

[27] Troch, P. and De Rouck, J., 1999. "An active wave generating-absorbing boundary condition for VOF type numerical model". *Coast. Eng.*, **38**, pp. 223–247.

[28] Carpenter, K.M, 1982. "Note on the paper 'Radiation conditions for the lateral boundaries of limited-area numerical models' by M.J. Miller, A.J. Thorpe." *Quart. J. R. Meteorol. Soc.*, **108**, pp. 717–719.

[29] Hagstrom, T. and Warburton, T., 2004. "A new auxiliary variable formulation of high-order local radiation boundary conditions: corner compatibility conditions and extensions to first-order systems". *Wave Motion*, **39**(4), pp. 327–338.

[30] Mar-Or, A. and Givoli, D., 2009. "High order global-regional model interaction: Extension of Carpenter's scheme". *Int. J. Numer. Meth. Eng.*, **77**, pp. 50–74.

[31] Mar-Or, A. and Givoli, D., 2010. "High-order one-way model nesting in dispersive non-uniform media". *J. Comput. Appl. Math*, **234**, pp. 1663–1669.

[32] Givoli, D. and Neta, B., 2003. "High-order non-reflecting boundary conditions for dispersive waves". *Wave Motion*, **37**(3), pp. 257–271.